A&A 490, 297–305 (2008)
DOI: 10.1051/0004-6361:200810260

Astronomy & Astrophysics

Spectroscopic metallicities of Vega-like stars⋆

C. Saffe[1,⋆⋆], M. Gómez[2], O. Pintado[3], and E. González[4]

[1] Complejo Astronómico El Leoncito, CC 467, 5400 San Juan, Argentina
e-mail: csaffe@casleo.gov.ar
[2] Observatorio Astronómico de Córdoba, Laprida 854, 5000 Córdoba, Argentina
e-mail: mercedes@oac.uncor.edu
[3] Instituto Superior de Correlación Geológica (INSUGEO), 4000 Tucumán, Argentina
e-mail: opintado@tucbbs.com.ar
[4] Facultad de Ciencias Exactas, Físicas y Naturales (UNSJ), 5400 San Juan, Argentina
e-mail: erip.p.a.gonzalez@gmail.com

Received 26 May 2008 / Accepted 1 August 2008

ABSTRACT

Aims. We aim to determine the metallicities of 113 Southern Hemisphere Vega-like candidate stars in relation to the giant exoplanet host group and field stars.
Methods. We applied two spectroscopic methods of abundance determinations: equivalent width measurements together with the ATLAS9 model atmospheres and the WIDTH9 program, and a comparison of observed spectra with a grid of synthetic spectra.
Results. For the Vega-like group, the metallicities are indistinguishable from those of field stars not known to be associated with planets or disks. This result is quite different from the metallicities of giant exoplanet host stars, which are metal-rich in comparison to field stars.

Key words. techniques: spectroscopic – stars: abundances – stars: late-type

1. Introduction

It is well established that stars with giant planets are, on average, metal-rich in comparison to stars that do not harbor Doppler-detected planets (see, for example, Santos et al. 2004). However, stars that have Neptune-mass planets do not seem to follow the same trend. In other words, Neptune-like or super-Earth planets do not form preferentially around metal-rich stars (e.g. Udry et al. 2006; Sousa et al. 2008). Two hypotheses have been put forward to explain the peculiar high metallicity of the giant exoplanet host stars: a) a primordial origin and b) a pollution of the convective zone of the star. In the first case the "excess" of metallicity was already present in the parent cloud from which the star-bearing planet was formed (see, for example, Santos et al. 2001). In the pollution scenario the convective zone of the star is contaminated by the infall or accretion of planets and/or planetesimals (see, for example, González et al. 2001).

Santos et al. (2004) found a lack of correlation between the thickness of the convective zone and the metallicity for a sample of FG dwarfs with planets. As the convective zone acts as a diluting medium, for a given amount of accreted material, F dwarfs with thinner convective zones should exhibit a greater degree of pollution than G dwarfs with thicker zones. On average, F and G dwarfs exhibit similar metallicities and the pollution hypothesis is not favored by these observations. The primordial origin of the "excess" remains an alternative to explain the relatively high metallicity of stars with giant planets with respect to field stars.

Pasquini et al. (2007) compared the metallicities of giant and dwarf stars with giant planets and found that the first group has, on average, lower metallicities than the dwarfs. The smaller mass of the convective zone of the dwarfs with respect to the giants provides a plausible explanation for this difference. The diluting effect of the convective zone is efficient for the giants and tends to lower the metallicity to its primordial value. In this case, the pollution scenario is favored (over the primordial origin) since it can explain the observed difference in metallicities between dwarfs and giants with planets. However, Hekker & Meléndez (2007) do not confirm Pasquini et al. result. In fact the first authors suggest that the metallicity enhancement of stars hosting giant planets might also be valid for giant stars. We note that the samples of stars in both cases are relatively small (14 objects in the case of Pasquini et al. and 20 for Hekker & Meléndez). The metallicity trend of giant stars with giant planets remains an open issue for the time being.

Even though the origin or the cause of the "excess" of metallicity of stars with giant planets is not well understood, these stars are metal-rich and this is a feature that distinguishes this group from stars with similar physical properties and no giant planets detected.

Vega-like stars are a group of objects that show infrared excesses in their spectral energy distributions that can be attributed to the presence of dust in circumstellar disks. The first members or candidate members of the class were selected by IRAS and had mainly A–F spectral types (Aumann et al. 1984; Gillett 1986; Backman & Paresce 1993; Sylvester et al. 1996; Mannings & Barlow 1998; Fajardo-Acosta et al. 1999; Sylvester & Mannings 2000; Habing et al. 2001; Laureijs et al. 2002; Sheret et al. 2004). Vega (αLyr) is one of the four proto-types of the group or the "fabulous four" (Vega, β Pictoris, Fomalhaut = α PsA and ϵ Eridanis; Gillett 1986) and has given the name to the class.

⋆ Tables 1–4 are only available in electronic form at http://www.aanda.org
⋆⋆ On a fellowship from CONICET, Argentina.

More recently, Spitzer has contributed to the detection of G dwarfs with infrared excesses (Meyer et al. 2004; Rieke et al. 2005; Kim et al. 2005; Chen et al. 2005; Uzpen et al. 2005; Beichman et al. 2005, 2006a; Bryden et al. 2006; Silverstone et al. 2006; Su et al. 2006; Trilling et al. 2008). Since the excesses come from distances similar to that of the Kuiper-Belt to the Sun, these stars have also received the designation of Kuiper-Belt analogs or Kuiper-Belt-like stars. In this paper we adopt the term "Vega-like stars" to refer to both IRAS and Spitzer detections.

The metallicity of Vega-like stars has previously been investigated by Greaves et al. (2006) and Chavero et al. (2006), deriving nearly solar values. However these works analyzed relatively small samples of objects. Greaves et al. (2006) studied a group of 18 FGK Vega-like stars whereas Chavero et al. (2006) included 42 FG dwarfs with infrared excesses in their metallicity determination. In addition these previous works do not include stars of A spectral type which represent the majority of IRAS detections. Greaves et al. (2006) derived their sample from the Doppler searches for planets that in general include solar type stars. Chavero et al. (2006) used Strömgren photometry to determine the metallicity. These works were also restricted to late spectral types.

Both stars with planets and the Vega-like stars have evidence of the presence of circumstellar material, in the form of planet/s, in the first case, or dust in a circumstellar disk, in the second. As mentioned before, the giant exoplanet hosts are metal-rich. This fact may have facilitated the formation of planets (Pollack et al. 1996). In this paper we determine spectroscopic metallicities of a large sample of Vega-like stars and compare our result with the exoplanet host group. We include objects of B–K spectral types, observable from the Southern Hemisphere.

2. The sample

We compiled a total of 113 Southern Hemisphere Vega-like candidate stars from the literature, based on their infrared or submillimetric excess emission (Backman & Paresce 1993; Sylvester et al. 1996; Mannings & Barlow 1998; Fajardo-Acosta et al. 1999; Sylvester & Mannings 2000; Habing et al. 2001; Laureijs et al. 2002; Sheret et al. 2004). This compilation also includes G dwarfs with infrared excess recently detected by Spitzer (Beichman et al. 2005, 2006a; Bryden et al. 2006; Su et al. 2006; Trilling et al. 2008). Specifically the list comprises objects with BAFGK spectral types (22, 38, 28, 17 and 8, respectively). All the stars are luminosity class V (Hipparcos catalogue) and have distances between 5 and 300 pc. Table 1 (available in the online version of the paper) lists the observed objects, including the $v \sin i$ values from the literature (Glebocki et al. 2000; Mora et al. 2001; Yudin 2001; Royer et al. 2002; Cutispoto et al. 2002, 2003; Pizzolato et al. 2003; Strom et al. 2005; Reiners 2006).

Table 1 includes a sub-sample of stars that were originally selected by IRAS as candidate Vega-like stars. However, when observed by Spitzer the infrared excesses were deemed to be of little significance. These objects are: HD 10800, HD 20794, HD 38393, HD 41700, HD 68456, HD 160691, HD 169830, HD 203608, and HD 216437 (Beichman et al. 2005, 2006a; Bryden et al. 2006; Hillenbrand et al. 2008; Trilling et al. 2008). For example, Bryden et al. (2006) found that for HD 10800 $\frac{f_{\mathrm{MIPS\_70\ mum}}}{f_*} = 1.3$ (the observed flux over the photospheric emission at 70 μm) and $\frac{f_{\mathrm{MIPS\_70\ mum}}}{f_*} = 1.2$ for HD 68456. This group of objects should be considered with caution.

3. Observations and data reduction

The stellar spectra were obtained at the Complejo Astronomico El Leoncito (CASLEO), using the *Jorge Sahade* 2.15-m telescope equipped with a REOSC echelle spectrograph[1] and a TEK 1024 × 1024 CCD detector. The REOSC spectrograph uses gratings as cross dispensers. We used a grating with 400 lines mm^{-1}, covering the spectral range $\lambda\lambda$3500–6500, giving a resolving power of ~12 500. Three individual spectra for each object were obtained in four observing runs: August 05–08, 2005, August 18–22, 2005, February 18–25, 2006 and May 04–07, 2007 and have S/N ratio of about 300.

The spectra were reduced using IRAF[2] standard procedures for echelle spectra. We applied bias and flat corrections and then normalized order by order with the *continuum* task, using 7–9 order Chebyshev polynomials. We also corrected the scattered light in the spectrograph (*apscatter* task). We fitted the background with a linear function on both sides of the echelle apertures, using the task *apall*. The resolution of the reduced spectra is 0.17 Å/pix.

4. Metallicity determinations

We used two different methods of abundance determination:

1) Fe line equivalent width measurements together with the ATLAS9 (Kurucz 1993) model atmosphere corresponding to a given star and the WIDTH9[3] program;
2) a comparison of the observed and synthetic spectra using the Downhill method (Gray et al. 2001). In particular we used the grid of synthetic spectra calculated by Munari et al. (2005). This method offers the advantage that there is no need to identify and measure the equivalent widths of many Fe lines as with the WIDTH9 program.

4.1. Metallicity determinations using the WIDTH program

To determine abundances by this method it is necessary to estimate the stellar parameters T_{eff} and $\log g$, by means of the Strömgren photometry, for example. With these quantities we adopt the Kurucz (1993) model atmosphere appropriate for each star. The model that initially is chosen has solar metallicity. Finally the Kurucz model together with the measured equivalent widths are used by the WIDTH9 program (Kurucz 1992, 1993) to derive the metallicity.

To obtain T_{eff} and $\log g$, we have used the *uvbyβ* mean colors of Hauck & Mermilliod (1998) with two different calibrations: Napiwotzki et al. (1993) and Castelli et al. (1997) and Castelli (1998) (hereafter N93 and C97, respectively), with the TEMPLOGG code (Rogers et al. 1995). This program has been used in the COROT mission preparation (see, for example, Lastennet et al. 2001; Guillon & Magain 2006) and includes reddening corrections, according to Domingo & Figueras (1999), for stars in the range A3–F0, and to Nissen (1988) for spectral types F0–G2.

We have compared the temperatures and gravities derived using both calibrations (N93 and C97) and noticed some differences, particularly in the later parameter. For this reason we

[1] On loan from the Institute d'Astrophysique de Liege, Belgium.
[2] IRAF is distributed by the National Optical Astronomical Observatories which is operated by the Association of Universities for Research in Astronomy, Inc., under a cooperative agreement with the National Science Foundation.
[3] http://kurucz.harvard.edu/programs.html

initially determined metallicities using values derived from both calibrations and later on considered if they significantly affect the final metallicity values. We have also compared the obtained $T_{\rm eff}$ with those published by Nordström et al. (2004). We found a good agreement, in particular with the N93 calibration. With the values of $T_{\rm eff}$ and log g derived for each object, we have chosen the corresponding model atmosphere using the Kurucz ATLAS9 (Kurucz 1993) code.

The stellar lines were identified using multiplet tables (Moore 1945), wavelengths and transition probabilities (Reader et al. 1980), as well as more specialized references for the Fe II lines (Johansson 1978). The Fe lines used are listed in the Table 2 (available in the online version of the paper), along with the corresponding log gf values from Fuhr et al. (1988) and Kurucz (1988, 1994). This list includes lines usually measured for early-type stars (e.g. Qiu et al. 2001; Saffe & Levato 2004) as well as solar-type stars (e.g. González 1998; González et al. 2001). The equivalent widths were measured by fitting Gaussian profiles through the stellar metallic lines using the IRAS *splot* task. There is no more than a 15% difference among the equivalent widths of the same line, measured in different spectra. We have excluded from our abundance determinations very blended lines.

To determine the abundances we need an initial estimation of the microturbulent velocity (ξ). For this estimation we have used the standard method. We computed the abundances from the Fe lines for a range of possible values of ξ satisfying two conditions: a) that the abundances of Fe lines is not dependent on the equivalent widths and b) that the rms errors are minima. To achieve the first condition the slope in the plot abundance vs. ξ must be zero. We tried different ξ values to fulfill this requirement. The final abundance value should fulfill both conditions a) and b). In this sense the abundance and microturbulent velocity determinations are recursive and simultaneous. Once a ξ value has been fixed the abundances corresponding to all chemical species measured are determined using the WIDTH9 code.

The WIDTH9 code requires the model atmosphere calculated by the ATLAS9 program, the equivalent width of each line as well as atomic constants such as oscillator strength (log gf) values, excitation potentials, damping constants, etc. This code calculates the theoretical equivalent widths for an initial input abundance and compares these values with the measured equivalent widths. Then the code modifies the abundance to achieve a difference between theoretical and measured equivalent widths <0.01 mÅ. The final values of the metallicities corresponding to the N93 and C97 calibrations, are listed in Table 3 (available in the online version of the paper). In this table we also include the fundamental stellar parameters $T_{\rm eff}$, log g and ξ, corresponding to each calibration, the slope of the plot [Fe/H] vs. equivalent width, the number of lines used in each determination, as well as the rms of the average.

To estimate errors for our WIDTH metallicities we consider the following facts. The most significant contribution to the final uncertainties probably comes from the equivalent width measurements. We assume a 5% error due to the continuum level determination. This translates into 20% maximum uncertainties in the metallicity estimation. The atomic constants may also have uncertainties. In particular we estimate that the oscillator strength values may cause differences of about 10% in the calculated metallicity. Finally to provide an estimation of "typical" errors introduced by the WIDTH method we increased the $T_{\rm eff}$ by 150 K and the log gf by 0.15, and recalculated the metallicity value for each star. We derived a median difference of 0.20 dex. The largest difference corresponds to HD 28 978 (0.55 dex).

4.2. Metallicity derivations from synthetic spectra: the Downhill method

The WIDTH method is not practical when the number of stars is large. For each object, we need to identify and measure many spectral lines. An alternative would be to compare the observed spectra with a grid of synthetic ones corresponding to different values of the metallicites and choose from the grid the spectrum that best reproduces the observed data (Gray et al. 2001). This comparison has the advantage that the complete profiles of the lines and not only the equivalent widths are used in the metallicity determinations.

In general synthetic spectra depend on four parameters: $T_{\rm eff}$, surface gravity (log g), metallicity ([Fe/H]) and microturbulent velocity (ξ). Following Gray et al. (2001), we applied a multidimensional Downhill Simplex technique, in which the observed spectrum is compared to a grid of synthetic spectra. The "final" synthetic spectrum is an interpolation of spectra, rather than a single point on the grid. As we are working with four variables ($T_{\rm eff}$, log g, [Fe/H] and ξ) the interpolation is done in 4D, minimizing the square differences in each wavelength (i.e., the χ^2 statistics). The stellar parameters are determined with a higher accuracy than the steps in the grid since they correspond to interpolated values.

The grid of synthetic spectra was taken from Munari et al. (2005). The parameter range covered by the grid is the following:

$$
\begin{aligned}
3500\ \mathrm{K} &< T_{\rm eff} < 40\,000\ \mathrm{K}, \text{ with steps of } 250\ \mathrm{K},\\
0.0\ \mathrm{dex} &< \log g < 5.0\ \mathrm{dex}, \text{ with steps of } 0.5\ \mathrm{dex},\\
-2.5\ \mathrm{dex} &< [\mathrm{Fe/H}] < 0.5\ \mathrm{dex}, \text{ with steps of } 0.5\ \mathrm{dex},\\
\text{and } \xi &\text{ values of } 0, 1, 2, \text{ and } 4\ \mathrm{km\,s^{-1}}.
\end{aligned}
$$

In addition to these parameters, the synthetic spectra are calculated for 15 different rotation velocities, ranging from 0–500 km s^{-1}. In all, Munari et al. (2005)'s library contains 625 000 different spectra. These authors calculated the complete synthetic spectral library for four resolving powers: 20 000, 11 500 (GAIA), 8500 (RAVE) and 2000 (SLOAN). Dr. U. Munari kindly provided a grid corresponding to the REOSC/CASLEO resolving power (12 500).

Synthetic spectral lines were convolved with the instrumental line profile corresponding to the REOSC/CASLEO. Finally they were also convolved with a Gaussian profile corresponding to the rotational velocities of the sample stars, taken from the literature (Glebocki et al. 2000; Mora et al. 2001; Yudin 2001; Royer et al. 2002; Cutispoto et al. 2002, 2003; Pizzolato et al. 2003; Strom et al. 2005; Reiners 2006). We weighted the synthetic spectra by the blaze function of each of the REOSC spectrograph orders. Finally we normalized and re-sampled our data to compare them with Munari et al. (2005)'s grid. The spectral sampling of the synthetic spectra is 0.02 Å.

We have implemented the Downhill method (Gray et al. 2001) by means of a Fortran program. From the stellar spectral type or the Strömgren photometry it is possible to estimate "a starting point" in the 4D grid. The Downhill method provides a searching algorithm within the 4D grid and finds the best match, minimizing the χ^2. In our case, the final spectrum is obtained by an interpolation of 16 spectra from Munari et al. (2005)'s grid. In general it takes 15–20 min for each star (50–60 iterations) with a Pentium IV 2.0 GHz processor to find the best interpolated spectrum. Table 4 (available in the online version of the paper) lists the metallicities obtained with the Downhill method for our sample of Vega-like stars.

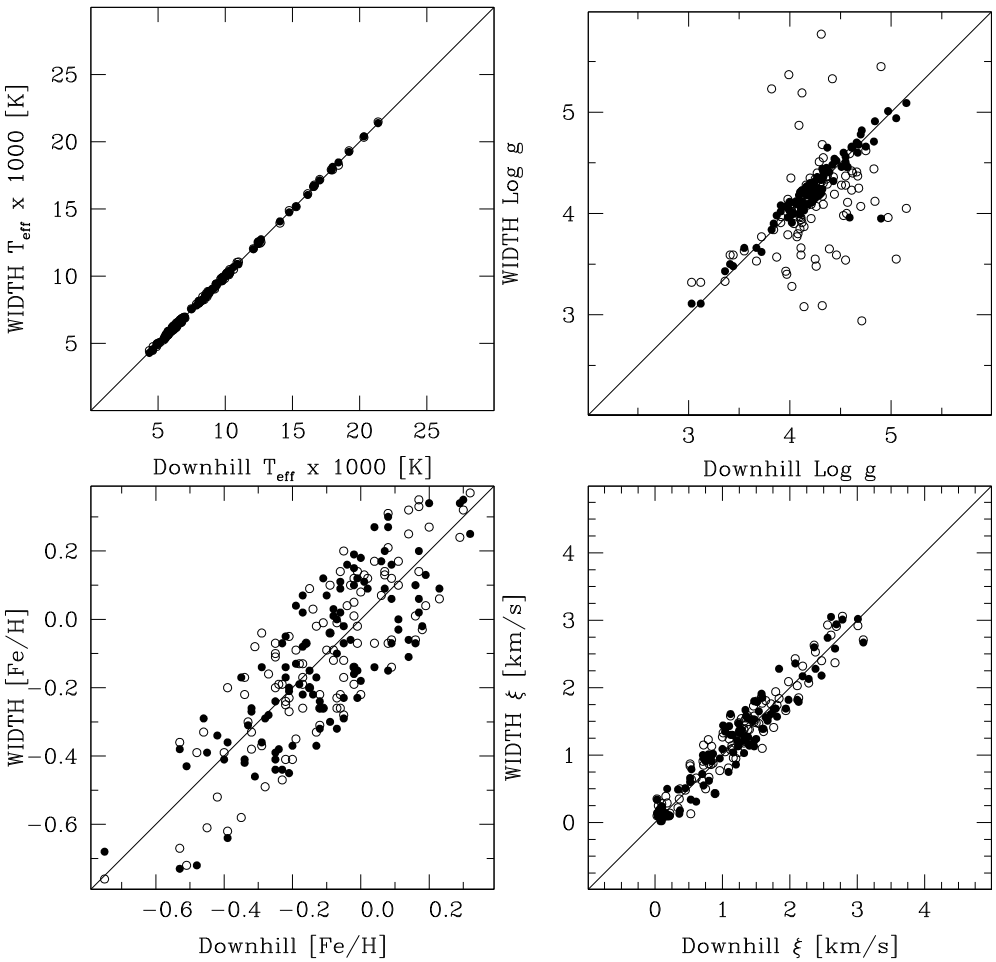

Fig. 1. Comparison of $T_{\rm eff}$, log g, [Fe/H], and ξ derived applying the Downhill and the WIDTH methods with the N93 and C97 calibrations. The x-axis show values derived from the Downhill and the y-axis the WIDTH determined parameters. With filled circles we indicate values obtained using the N93 calibration. The empty circles correspond to the C97 photometric relation. In the case of the $T_{\rm eff}$ plot (*upper-left panel*), values obtained from both calibrations are almost superimposed.

To estimate the uncertainties in the metallicities obtained by the Downhill method, we carried out a few tests. We first applied this method to 30 synthetic spectra of known metallicities. The median difference between the derived and known metallicities is 0.02 dex.

The internal consistency of the method has been checked by fixing one of the four variables and comparing the resultant metallicities. Fixed values for each variable were obtained, for example, from an adopted calibration:

a) $T_{\rm eff}$ was taken from the N93 calibration;

b) log g was adopted from the N93 calibration;

c) ξ was fixed at 2.9 km s^{-1}, the solar value.

The median difference, calculated by fixing 3 of the 4 variables with respect to the "standard" procedure (i.e., with 4 variables), was 0.05 dex. Considering this value and the median difference derived from the comparison with 30 synthetic spectra of known metallicities (0.02 dex), we estimate a "typical" uncertainty of $(0.02^2 + 0.05^2)^{-1/2} \sim 0.06$ dex for the metallicities derived by the Downhill method.

We finally mention two parameters taken as fixed by the Downhill method, the radial and the rotational velocities. Radial velocities are initially determined minimizing the χ^2 with an accuracy of 0.1 km s^{-1} or a median value of 0.03 dex in metallicity. Rotational velocities (v sin i) from the literature have "typical" dispersions of 5–10%, corresponding to an error of about 10% in metallicity.

In summary, we have estimated an internal uncertainty of 0.06 dex for metallicities derived from the Downhill method. A more conservative estimation would indicate a value of 0.1 dex. This corresponds to half of the uncertainty calculated for the WIDTH method (0.2 dex). In this manner, the Downhill method allows a more precise determination of the metallicities for our sample of Vega-like objects.

4.3. Comparison of metallicity determinations by the WIDTH and the Downhill methods

As mentioned in the previous section we used two calibrations (N93 and C97) with the WIDTH and the Downhill methods. In Fig. 1 we compare the corresponding values of $T_{\rm eff}$, log g, [Fe/H], and ξ. The x-axis shows the Downhill derived values and the y-axis the WIDTH determinations. In this case filled circles indicate values obtained applying the N93 calibration, while open circles the C97 relation. In general we find a good agreement with the exception of the log g values. In addition the log g Downhill method derived values agree better with those obtained with the WIDTH method and the N93 calibration rather than

Table 5. Medians and dispersions of the metallicities for the Vega-like sample.

Method	Median [Fe/H]	Dispersion [Fe/H]	N
WIDTH+N93	−0.14	0.28	113
WIDTH+C97	−0.11	0.26	113
Downhill	−0.11	0.27	113

Note – N93: Napiwotzki et al. (1993)'s calibration; C97: Castelli et al. (1997) and Castelli (1998)'s calibration.

with those determined with the WIDTH and the N97 photometric relation.

Table 5 lists the medians and the dispersions of the metallicities derived by applying the WIDTH and the Downhill methods for the Vega-like group. In the case of the WIDTH method we present the results corresponding to the two calibrations used (N93 and C97). The derived median values are practically indistinguishable.

Figure 2 compares the metallicity distributions calculated with the WIDTH method plus the N93 calibration (histogram shaded at 0 degrees) and the C97 calibrations (histogram shaded at 45 degrees), respectively. The empty histogram shows the distribution derived with the Downhill method for the Vega-like sample. Vertical lines indicate the medians of each distribution. The left line corresponds to the WIDTH+N93 median, and the right line shows (superimposed) the WIDTH+C97 and Downhill medians (see Table 5). The KS-test (Press 1992) indicates that these distributions are similar and represent the same parent population.

We finally adopt the metallicities calculated with the Downhill method for the sample of Vega-like stars, as these determinations use the complete line profiles and not only the equivalent widths. In addition "typical" uncertainties are smaller than those estimated for the WIDTH method.

Figure 3 shows the $T_{\rm eff}$, log g, [Fe/H] and ξ values derived in the present contribution (x axis) and those obtained from the literature (y axis). In particular we compare our determinations with the four recent works. The open squares correspond to Santos et al. (2004, 2005), filled circles to Nordström et al. (2004), empty circles to Fischer & Valenti (2005), and crosses to Sousa et al. (2008). We note a general good agreement although we also find a moderate dispersion between our determinations and those from the literature. We find no obvious systematic tendencies, except for 0.09 dex in [Fe/H] between our estimations and the Fischer & Valenti (2005) data.

We also noticed a systematic difference of ~0.09 dex between the Nordström et al. (2004) and Fischer & Valenti (2005) determinations. The Fischer & Valenti (2005) determinations are, on average, larger than those from Nordström et al. (2004). Our Downhill method derived metallicities show a better agreement with the Nordström et al. (2004) values than with Fischer & Valenti (2005). However this later comparison is based on a relatively small number of common stars. Our sample has 24 objects in common with Fischer & Valenti (2005) and 51 with Nordström et al. (2004). In the work of Nordström et al. (2004) the metallicities are derived as a secondary parameter obtained photometrically. In the case of Fischer & Valenti (2005), the metallicities are obtained by a comparison with synthetic spectra but using only a small range of wavelengths (6000–6200 Å).

The works of Santos et al. (2004, 2005) and Sousa et al. (2008) are based on high-signal to-noise spectra covering a wide spectral range. We find a reasonably good agreement with these

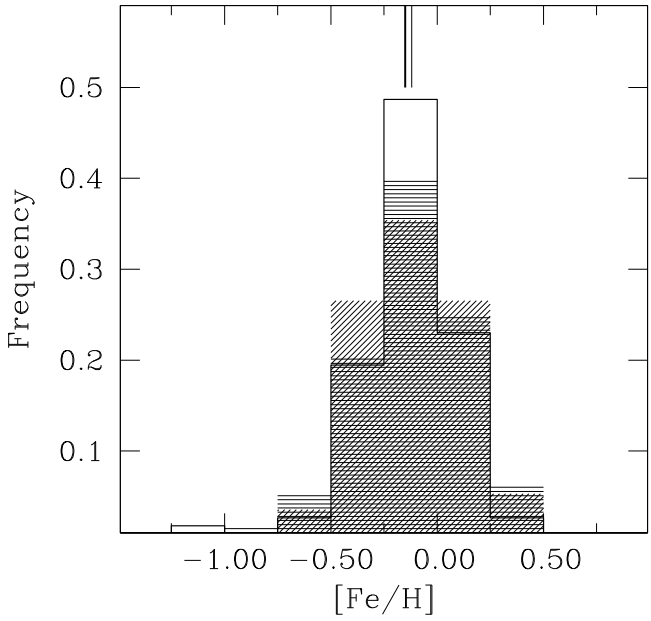

Fig. 2. Metallicity distributions for the Vega-like sample. Histograms shaded at 0 and 45 degrees correspond to the WIDTH method derivations using N93 (Napiwotzki et al. 1993) and C97 (Castelli et al. 1997; Castelli 1998) calibrations, respectively. The empty histogram shows the metallicity distribution derived by the Downhill method. The vertical lines indicate the medians of each distribution. The left line corresponds to the WIDTH+N93 median, and the right line shows (superimposed) the WIDTH+C97 and Downhill medians (see Table 5).

determinations. However this comparison is based on a limited number of common stars: 17 and 12 objects, respectively. Our metallicity values show a slightly better agreement with the Santos et al. data than with the Sousa et al. determinations. In summary, with these limitations and those mentioned in the cases of Nordström et al. (2004) and Fischer & Valenti (2005) in mind, we consider that the external consistency of the Downhill method derived metallicities is acceptable.

Lines with large equivalent widths are sensitive to NLTE effects. An attempt to analyze such lines in the LTE approach could lead to abundance overestimations, simply due to overestimation of the equivalent widths (e.g. Takeda 1992; Thevenin & Idiart 1999). In general, equivalent width overestimations become more severe at low temperatures. In addition an apparent systematic difference of abundances between high and low excitation FeI lines ($[{\rm Fe/H}]_{\rm high} > [{\rm Fe/H}]_{\rm low}$) has been attributed to NLTE effects (e.g. Takeda 1992; Ruland et al. 1980). We find no systematic dependence of the WIDTH LTE derived metallicities (and dispersions) on the excitation potential for the stars in our sample, or the atmospheric stellar parameters. Consequently the metallicity scale seems to be constant for all the stars in our sample. However this does not completely rule out NLTE effects. Our LTE calculations, nevertheless, allow us to compare our derivations with most previous works in the literature, which make similar LTE assumptions.

5. Discussion of the results

The metallicity of the Solar Neighborhood is usually represented by a control sample of stars, which should exclude, in our case, known Vega-like stars. The selection of the control sample is important, because different groups of objects (i.e., stars selected by different criteria) may have different metallicities. For

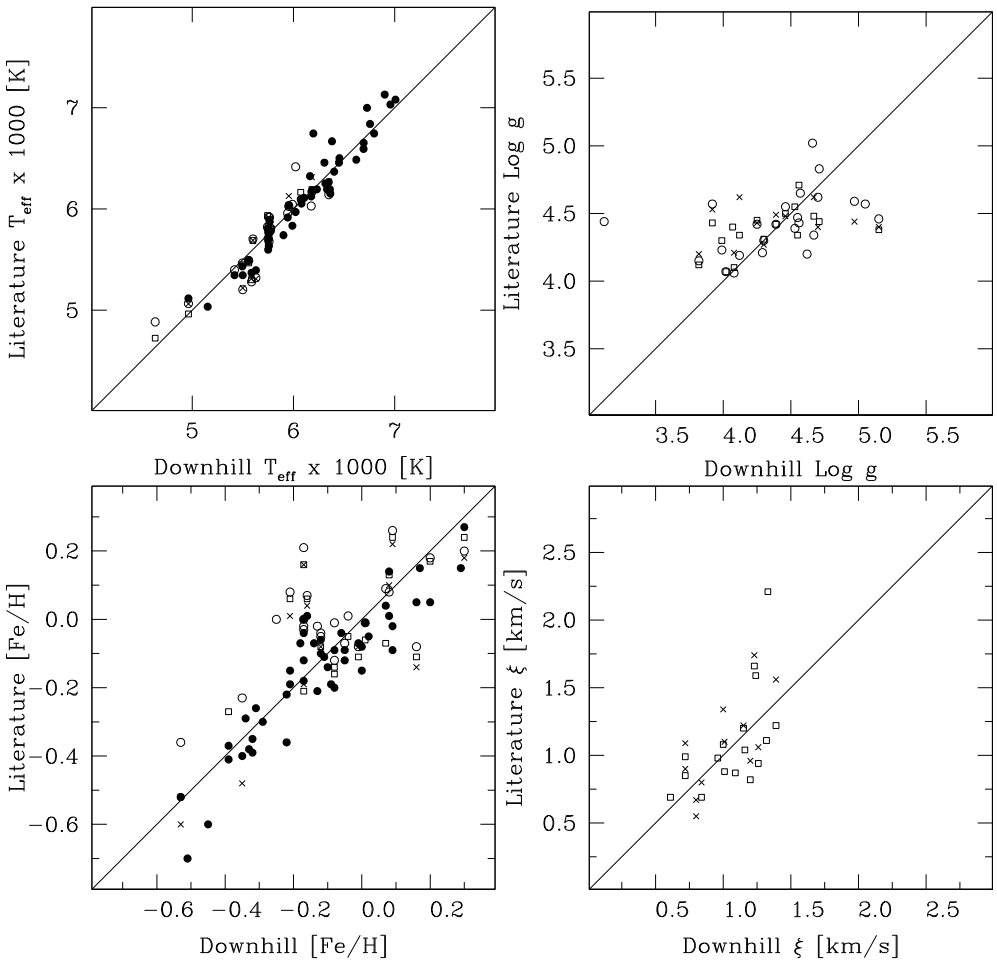

Fig. 3. Comparison of $T_{\rm eff}$, log g, [Fe/H] and ξ derived in this contribution (x axis) with those obtained from the literature (y axis). The open squares correspond to Santos et al. (2004, 2005), filled circles to Nordström et al. (2004), empty circles to Fischer & Valenti (2005), and crosses to Sousa et al. (2008).

example, Fischer & Valenti (2005) compared two different control samples, with the metallicity distribution of exoplanet host stars. Their control sets are volume-limited and magnitude-limited. The medians of the metallicity "excess" of the giant exoplanet host stars compared with the two groups are 0.13 and 0.226 dex, respectively. In other words, the "excess" is real, but the amount depends on the control sample used. The two control sets contain different classes of stars. The magnitude-limited sample includes more massive and metal-rich stars than the volume-limited set.

The metallicity distribution of exoplanet host stars is usually compared with a volume-limited group of solar neighborhood stars (González 1998, 1999; González et al. 2001; Santos et al. 2000, 2003, 2004; Sadakane et al. 2002; Laws et al. 2003). We compared the metallicity distribution of our Vega-like sample with a volume-limited sample of 71 stars, without Doppler detected exoplanets (Santos et al. 2001; Gilli et al. 2006) and with 98 exoplanets host stars (Santos et al. 2004). Metallicity values for these two comparison samples were obtained from Nordström et al. (2004). As discussed in Sect. 4.2, the agreement between our metallicities and those obtained by these authors is acceptable. Figure 4 shows these distributions. Vega-like stars are represented by the empty histogram, stars with giant planets by the histogram shaded at 0 degrees and stars known not to harbor planets detected by the Doppler technique, by the histogram shaded at 45 degrees. The KS test shows no significant difference between the metallicity distributions of the Vega-like stars and stars without planets. On the other hand, the Vega-like stars metallicity distribution is different from the metallicity distribution for stars with giant planets, with a high level of confidence.

Fischer & Valenti (2005) obtained that the probability that a FGK star harbors a giant planet/s increases as $P(Z) \propto (10^Z)^2$, where Z is the stellar metallicity (see also, Wyatt et al. 2007b). If this relation is also applicable to A stars (the bulge of IRAS detected Vega-like stars), the low median value of the metallicity for the Vega-like group (−0.11 dex, see Table 6) indicates that the probably of these stars hosting a planet/s of the type detected by radial velocity surveys is also low. We note, however, that the dispersion of metallicities within the Vega-like stars is also significant (0.26 dex) and at least a fraction of these stars has metallicities high enough to host giant planets, assuming the "excess" of metallicity/presence of a giant planet/s holds for A spectral type stars. In addition Doppler searches do not achieve the required precision to detect giant planets in A stars as metal lines practically disappear.

We also compared the metallicity distribution of Vega-like stars with a sample of 115 stars without excess at 24 or 70 μm, observed by Spitzer (Beichman et al. 2005, 2006a; Bryden et al. 2006; Su et al. 2006). The metallicities of these stars were taken from literature (Sousa et al. 2008; Santos et al. 2004, 2005; Nordström et al. 2004). Figure 5 shows these distributions. Vega-like stars are indicated by the empty histogram whereas the stars without excess at 24 or 70 μm are shown by the histogram shaded at 45 degrees. The KS test shows no significant difference

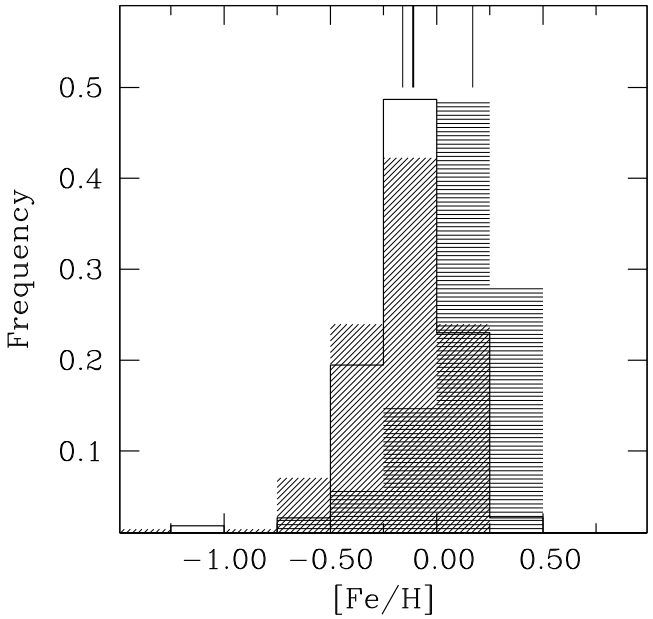

Fig. 4. Metallicity distributions for the Vega-like sample, empty histogram, for stars with giant planets, histogram shaded at 0 degrees, and for stars known not to harbor planets, histogram shaded at 45 degrees. The vertical lines indicate the medians of each distribution: stars without planets, Vega-like stars, and exoplanet host stars, respectively (see Table 6).

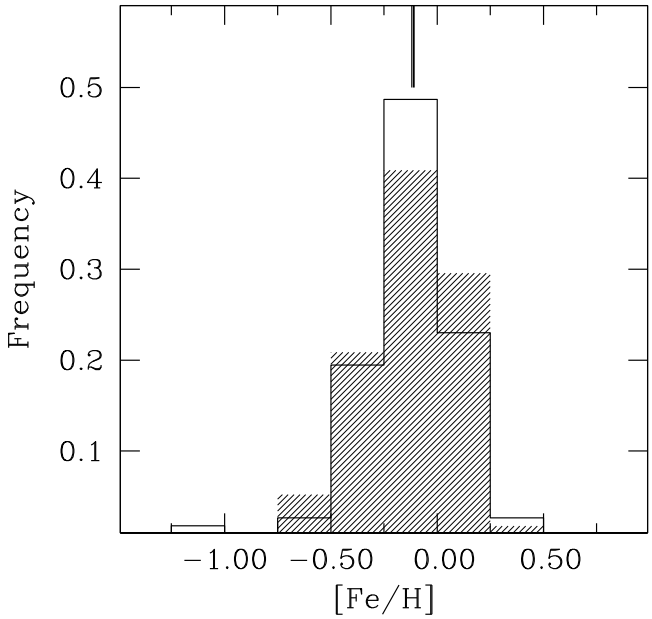

Fig. 5. Metallicity distributions for the Vega-like sample, empty histogram, and for stars without excess at 24 or 70 μm (Beichman et al. 2005, 2006a; Bryden et al. 2006; Su et al. 2006). The vertical lines (almost superimposed) indicate the medians of each distribution.

Table 6. Medians and dispersions of the Vega-like sample and three comparison groups.

Sample	Median [Fe/H]	Dispersion [Fe/H]	N
Vega-like stars	−0.11	0.27	113
Exoplanet host stars	+0.17	0.22	98
Volume-limited sample without planets	−0.16	0.25	71
Stars without excess at 24 or 70 μm	−0.12	0.24	115

between the two distributions. Table 6 lists the medians and the dispersions of the four samples compared in Figs. 4 and 5.

The results in Table 6 indicate that, on average, the Vega-like group has metallicities similar to the stars in the Solar Neighborhood without detected planets or disks, in contrast to the giant exoplanet host stars group. This result confirms and extends previous works by Greaves et al. (2006) and Chavero et al. (2006), based on relatively small numbers of FG Vega-like stars.

In Fig. 6 we analyze the metallicity distribution of Vega-like stars of different spectral types. The number of objects corresponding to each spectral type is indicated between brackets. The vertical bars are the dispersions within the spectral types. A-spectral-type stars still dominate the Vega-like group although Spitzer has significantly contributed F and G stars during the last few years (Beichman et al. 2005, 2006a; Bryden et al. 2006; Su et al. 2006). Figure 6 shows no trend of metallicity with spectral type for the Vega-like group.

As suggested by Greaves et al. (2006) the relatively high metallicity of giant exoplanet host stars as well as the solar metallicity value for the Vega-like stars can be understood within the core accumulation model of Pollack et al. (1996). The high

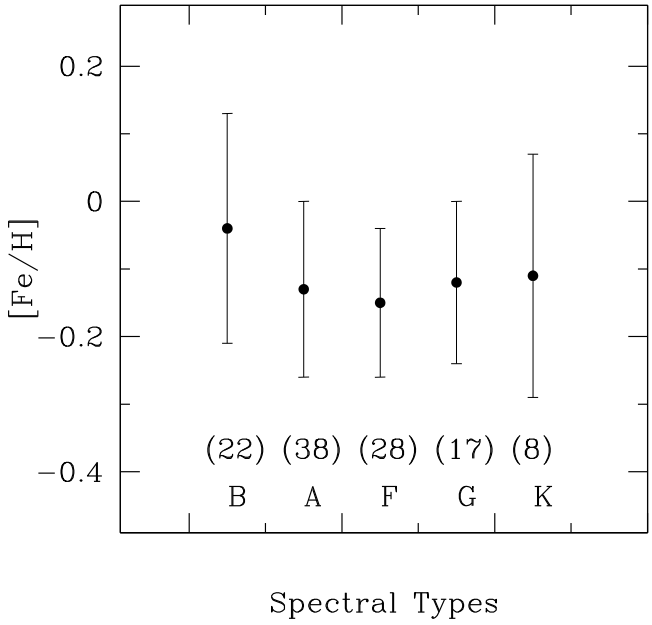

Fig. 6. Metallicity of Vega-like stars of different spectral types. Between brackets is indicated the number of objects in each spectral type bin. The vertical lines are the corresponding dispersions.

metal content of the disk favors the fast formation of giant planets, which needs to accrete an atmosphere and migrate inward before the gas is dissipated from the disk. On the contrary, for Vega-like objects no giant planet needs to be formed and/or migrate inward. The gas may dissipate and still the planetesimal in the external part of the disk may produce dust by collisions.

We tentatively analyzed two small sub-sets of Vega-like objects: the Vega-like stars with giant planets and the Vega-like group with no Doppler detected giant planets. The first group is composed of 7 stars: 6 with 70 μm excess detected by Spitzer (HD 33636, HD 50554, HD 52265, HD 82943, HD 128311 and

HD 117176; Beichman et al. 2006a) and ϵ Eri with infrared and submillimieter excesses (Greaves et al. 1998; Zuckerman 2001). In the second group we include 5 stars without giant exoplanets detected by the Doppler technique (Santos et al. 2004; Gilli et al. 2006) and showing infrared excess in 24 or 70 μm (HD 7570, HD 38858, HD 69830, HD 76151 and HD 115617; Beichman et al. 2006a; Bryden et al. 2006). HD 69830 is included in the second group since it harbors 3 Neptune- or super-Earth-mass planets (Lovis et al. 2006).

The median metallicity of Vega-like stars with planets is +0.07 dex and the dispersion is 0.16 dex. For the Vega-like objects without planets these values are: −0.08 and 0.18 dex, respectively. It seems that when a Vega-like star has a giant planet the metallicity increases slightly. However the small number of objects available as well as the dispersions prevent us from giving any statistical significance to this initial trend.

Greaves et al. (2007) proposed that the solid-mass (i.e., metal) content in primordial disks, called M_S, is the fundamental parameter that regulates the planet/disk formation. If M_S is small, the star will form a Vega-like disk, while if M_S is larger, a giant planet may be formed. Table 1 of Greaves et al. (2007) shows the range of metallicity and the final configurations (planet+debris, debris, etc.) derived by these authors. The medians of the metallicities of Vega-like stars with and without planets agree with Greaves et al. (2007)'s Table 1. However this can only be considered as an initial trend that needs to be confirmed by increasing the number of Vega-like objects with planets as well as objects known not to harbor Doppler detected planetary mass objects.

Finally, the stellar mass may also play an important role in the occurrence of giant planets. This type of planet seem to be more frequent in intermediate-mass than in low-mass stars (Johnson et al. 2007). Using radial velocity, Lovis & Mayor (2007) discovered a giant planet orbiting an open cluster star (NGC 2423, No. 3) with 2.4 $M_\odot$. Johnson et al. (2008) reported the detection of two giant planets orbiting two intermediate-mass mass stars (1.80 and 1.64 $M_\odot$, respectively), discovered as part as their survey of evolved stars.

6. Summary and conclusions

We derived spectroscopic metallicities for a group of 113 Southern Hemisphere Vega-like stars. We applied two methods to determine metallicities: the "classical" WIDTH method and a comparison with the grid of synthetic spectra of Munari et al. (2005) by means of the Downhill algorithm. The later method offers the advantage that the complete profile of the line is used in the metallicity derivation and not only the equivalent width. In addition we estimated smaller uncertainties in the metallicities derived by the Downhill method (0.1 dex) than with the WIDTH code (0.2 dex).

Vega-like stars have metallicities similar to Solar Neighborhood stars without planets or disks and significantly different to the giant exoplanet host stars. This result confirms previous estimations by Greaves et al. (2006) and Chavero et al. (2006), based on comparatively smaller samples.

The low metallicities for the Vega-like group (median = −11 dex) in relation to the exoplanet host stars (median = +0.17 dex, Santos et al. 2004) may indicate that the probability of these stars hosting a giant planet/s of the type detected by radial velocity surveys is also low. However the dispersion of metallicities within the Vega-like stars is also significant (0.26 dex) and thus a fraction of these objects may have metallicities high enough to form giant planets. We caution that exoplanet host stars are mainly of FGK spectral types whereas the bulge of IRAS detected Vega-like stars has A spectral type which are, in general, excluded from radial velocity searches since high precisions are not feasible. In this we are assuming that the probability of an A star being associated with a giant planet depends on the metallicity, as is the case for FGK stars.

We find no trend in the metallicities of Vega-like objects with the spectral type. The Greaves et al. (2006) suggestion makes compatible the relatively high metallicity of giant exoplanet host stars and the solar neighborhood value for Vega-like stars with the core accumulation model of Pollack et al. (1996).

Analyzing two relatively small sub-samples, we find that Vega-like stars with a Doppler detected planet have slightly higher metallicities than Vega-like stars known not to harbor such a planet. However this must be considered only as an initial trend that needs to be confirmed by increasing both samples to achieve a statistically significant result.

Acknowledgements. The authors thank Drs. F. Castelli, P. Bonifacio and L. Sbordone for making their codes available to them.

References

Aumann, H. H., Beichman, C. A., Gillett, F. C., et al. 1984, ApJ, 278, 23
Apai, D., Janson, M., Moro-Martin, A., et al. 2008, ApJ, 672, 1196
Backman, D. E., & Paresce, F. 1993, in Protostars and planets III, ed. E. H. Levy, J.I. Lunine, & M. S. Mathews (Tucson: Univ. Arizona Press), 1253
Beichman, C. A., Bryden, G., Rieke, G. H., et al. 2005, ApJ, 622, 1160
Beichman, C. A., Bryden, G., Stapelfeldt, K. R., et al. 2006a, ApJ, 652, 1674
Beichman, C. A., Tanner, A., Bryden, G., et al. 2006b, ApJ, 639, 1166
Bryden, G., Beichman, C. A., Trilling, D. E., et al. 2006, ApJ, 636, 1098
Castelli, F. 1998, Mem. Soc. Astron. Ital., 69, 165
Castelli, F., Gratton, R. G., & Kurucz, R. L. 1997, A&A, 318, 841
Chavero, C., Gómez, M., Whitney, B. A., & Saffe, C. 2006, A&A, 452, 921
Chen, C. H., Patten, B. M., Werner, M. W., et al. 2005, ApJ, 634, 1372
Chen, C. H., Sargent, B. A., Bohac, C., et al. 2006, ApJS, 166, 351
Cheng, K. P., Bruhweiler, F. C., Kondo, Y., & Grady, C. A. 1992, ApJ, 396, 83
Clampin, M., Krist, J. E., Ardila, D. R., et al. 2003, AJ, 126, 385
Cote, J. 1987, A&A, 181, 77
Cutispoto, G., Pastori, L., Pasquini, L., et al. 2002, A&A, 384, 491
Cutispoto, G., Tagliaferri, G., de Medeiros, J. R., et al. 2003, A&A, 397, 987
Decin, G., Dominik, C., Waters, L. B. F. M., & Waelkens, C. 2003, ApJ, 598, 636
Fajardo-Acosta, S. B., Stencel, R. E., Backman, D. E., & Thakur, N. 1999, ApJ, 520, 215
Fischer, D. A., & Valenti, J. A. 2005, ApJS, 622, 1102
Friedemann, C., Guertler, J., & Loewe, M. 1996, A&AS, 117, 205
Fuhr, J. R., Martin, G. A., & Wiese, W. L. 1988, Atomic transition probabilities, Scandium through Manganese, New York: Amer. Instit. Phys. (AIP) and American Chemical Society
Gillett, F. C. 1986, in Light on dark matter; Proceedings of the First Infrared Astronomical Satellite Conference, Noordwijk, Netherlands, June 10–14, 1985 (A87-11851 02-90) (Dordrecht: D. Reidel Publishing Co.), 61
Gillon, M., & Magain, P. 2006, A&A, 448, 341
Domingo, A., & Figueras, F. 1999, A&A, 343, 446
Gilli, G., Israelian, G., Ecuvillon, A., Santos, N. C., & Mayor, M. 2006, A&A, 449, 723
Glebocki, R., & Stawikowski, A. 2000, Acta Astron., 50, 509
González, G. 1998, A&A, 334, 221
González, G. 1999, MNRAS, 308, 447
González, G., Laws, C., Tyagi, S., & Reddy, B. E. 2001, AJ, 121, 432
Gray, R. O., Graham, P. W., & Hoyt, S. R. 2001, AJ, 121, 2159
Greaves, J. S., Holland, W. S., Moriarty-Schieven, G., et al. 1998, ApJ, 506, 133
Greaves, J. S., Fischer, D. A., & Wyatt, M. C. 2006, MNRAS, 366, 283
Greaves, J. S., Fischer, D. A., Wyatt, M. C., Beichman, C. A., & Bryden, G. 2007, MNRAS, 378, L1
Habing, H. J., Dominik, C., Jourdain de Muizon, M., et al. 2001, A&A, 365, 545
Hauck, B., & Mermilliod, M. 1998, A&AS, 129, 431
Hekker, S., & Meléndez, J. 2007, A&A, 475, 1003
Hillenbrand, L. A., Carpenter, J. M., Kim, J. S., et al. 2008, ApJ, 677, 630
Holland, W. S., Greaves, J. S., Zuckerman, B., et al. 1998, Nature, 392, 788
Jaschek, M., Jaschek, C., & Egret, D. 1986, A&A, 158, 325
Johansson, S. 1978, Phys. Scrip., 18, 217
Johnson, J. A., Fischer, D. A., Marcy, G. W., et al. 2007, ApJ, 665, 785

Johnson, J. A., Marcy, G. W., Fischer, D. A., et al. 2008, ApJ, 675, 784
Jura, M., Chen, C. H., Furlan, E., et al. 2004, ApJS, 154, 453
Kim, J. S., Hines, D. C., Backman, D. E., et al. 2005, A&A, 632, 659
Kurucz, R. L. 1988, Trans. IAU, XXB, ed. M. McNally (Dordrecht: Kluwer), 168
Kurucz, R. L. 1992, Rev. Mex. Astron. Astrofis., 23, 45
Kurucz, R. L. 1993, ATLAS, Stellar Atmosphere Programs and 2 km s^{-1} grid, Kurucz CM-ROM No. 13, Smithsonian Astrophysical Observatory, Cambridge, MA
Kurucz, R. L. 1994, ATLAS Atomic Data for Fe and Ni, Kurucz CM-ROM No. 22, Smithsonian Astrophysical Observatory, Cambridge, MA
Lastennet, E., Lignies, F., Buser, R., et al. 2001, The Journal of Astronomical Data, 7
Laureijs, R. J., Jourdain de Muizon, M., Leech, K., et al. 2002, A&A, 387, 285
Laws, C., González, G., Walker, K. M., et al. 2003, AJ, 125, 2664
Lovis, C., & Mayor, M. 2007, A&A, 472, 657
Lovis, C., Mayor, M., Pepe, F., et al. 2006, Nature, 441, 305
Mamajek, E. E., Hines, D. C., Backman, D. E., et al. 2005, A&AS, 207, 6348
Mannings, V., & Barlow, M. J. 1998, ApJ, 497, 330
Meyer, M. R., Hillenbrand, L. A., Backman, D. E., et al. 2004, ApJS, 154, 422
Moore, C. E. 1945, A multiplet table of astrophysical interest, Princeton, N.J., The Observatory, Rev. ed.
Mora, A., Merín, B., Solano, E., et al. 2001, A&A, 378, 116
Munari, U., Sordo, R., Castelli, F., & Zwitter, T. 2005, A&A, 442, 1127
Napiwotzki, R., Schoenberner, D., & Wenske, V. 1993, A&A, 268, 653
Nissen, P. E. 1988, A&A, 199, 146
Nordström, B., Mayor, M., Andersen, J., et al. 2004, A&A, 418, 989
Oudmaijer, R. D., van der Veen, W. E. C. J., Waters, L. B. F. M., et al. 1992, A&AS, 96, 625
Pascucci, I., Gorti, U., Hollenbach, D., et al. 2006, ApJ, 651, 1177
Pasquini, L., Döllinger, M. P., Weiss, A., et al. 2007, A&A, 473, 979
Patten, B. M., & Willson, L. A. 1991, AJ, 102, 323
Pizzolato, N., Maggio, A., Micela, G., Sciortino, S., & Ventura, P. 2003, A&A, 397, 147
Press, W. H., Teukolsky, S. A., Vetterling, W. T., & Flannery, B. P. 1992, Numerical Recipes in Fortran: The Art of Scientific Computing (Cambridge University Press), 2nd edition, 617
Pollack, J. B., Hubickyj, O., Bodenheimer, P., et al. 1996, Icarus, 124, 62
Qiu, H. M., Zhao, G., Chen, Y. Q., & Li, Z. W. 2001, ApJ, 548, 953
Reader, J., Corliss, C. H., Wiese, W. L., & Martin, G. A. 1980, Wavelengths and transition probabilities for atoms and atomic ions – Part 1: Wavelengths, National Standard Reference Data Series (NSRDS-NBS), Washington: National Bureau of Standards (NBS)
Reiners, A. 2006, A&A, 446, 267
Rieke, G. H., Su, K. Y. L., Stansberry, J. A., et al. 2005, ApJ, 620, 1010
Rogers, N. Y. 1995, Comm. Asteroseism., 78
Royer, F., Gerbaldi, M., Faraggiana, R., & Gómez, A. E. 2002, A&A, 381, 105
Ruland, F., Biehl, D., Holweger, H., & Griffin, R. 1980, A&A, 92, 70
Sadakane, K., & Nishida, M. 1986, PASP, 98, 685
Sadakane, K., Ohkubo, M., Takeda, Y., et al. 2002, PASJ, 54, 911
Saffe, C., & Levato, H. 2004, A&A, 418, 1083
Santos, N. C., Israelian, G., & Mayor, M. 2000, A&A, 363, 228
Santos, N. C., Israelian, G., & Mayor, M. 2001, A&A, 373, 1019
Santos, N. C., Israelian, G., Mayor, M., Rebolo, R., & Udry, S. 2003, A&A, 398, 363
Santos, N. C., Israelian, G., & Mayor, M. 2004, A&A, 415, 1153
Santos, N. C., Israelian, G., Mayor, M., et al. 2005, A&A, 437, 1127
Schneider, G., Silverstone, M. D., Hines, D. C., et al. 2006, ApJ, 650, 414
Sheret, I., Ramsay Howat, S. K., & Dent, W. R. F. 2003, MNRAS, 343, 65
Sheret, I., Dent, W. R. F., & Wyatt, M. C. 2004, MNRAS, 348, 128
Silverstone, M. D., Meyer, M. R., Mamajek, E. E., et al. 2006, ApJ, 639, 1138
Stencel, R. E., & Backman, D. E. 1991, ApJS, 75, 905
Song, I., Caillault, J.-P., Barrado y Navascués, D., & Stauffer, J. R. 2001, ApJ, 546, 352
Sousa, S. G., Santos, N. C., Mayor, M., et al. 2008, A&A, in press
Strom, S. E., Wolff, S. C., & Dror, D. H. A. 2005, ApJ, 129, 809
Su, K. Y. L., Rieke, G. H., Stansberry, J. A., et al. 2006, ApJ, 653, 675
Sylvester, R. J., & Mannings, V. 2000, MNRAS, 313, 73
Sylvester, R. J., Skinner, C. J., Barlow, M. J., & Mannings, V. 1996, MNRAS, 279, 915
Takeda, Y. 1992, A&A, 253, 487
Telesco, C. M., Fisher, R. S., Piña, R. K., et al. 2000, ApJ, 530, 329
Thevenin, F., & Idiart, T. P. 1999, ApJ, 521, 753
Trilling, D. E., Bryden, G., Beichman, C. A., et al. 2008, ApJ, 674, 1086
Udry, S., Mayor, M., Benz, W., et al. 2006, A&A, 447, 361
Uzpen, B., Kobulnicky, H. A., Olsen, K. A. G., et al. 2005, ApJ, 629, 512
Walker, H. J., & Wolstencroft, R. D. 1988, PASP, 100, 1509
Waters, L. B. F. M., van den Ancker, M. E., Baas, F., et al. 1995, A&A, 299, 173
Wyatt, M. C., Smith, R., Su, K. Y. L., et al. 2007a, ApJ, 663, 365
Wyatt, M. C., Clarke, C. J., & Greaves, J. S. 2007b, MNRAS, 380, 1737
Yudin, R. V. 2001, A&A, 368, 912
Zuckerman, B. 2001, A&ARv, 39, 549

Table 1. Sample of Vega-like stars observed at the CASLEO.

Star	Distance [pc]	V	$v \sin i$ [km s^{-1}]	Spectral type	Reference
HD 105	40	7.51	14.5	G0V	DEC03 HILL08
HD 142	26	5.70	11.0	G1V	BE05 TR08
HD 2623	365	7.93	9.0	K2	SB91
HD 3003	46	5.07	10.4	A0V	MB98 O92 SB91 WY07
HD 9672	61	5.62	19.3	A1V	MB98 O92 SB91 PW91 WW88 SN86 WY07
HD 10647	17	5.52	5.5	F8V	MB98 O92 SB91 DEC03 TR08
HD 10700	4	3.49	5.9	G8V	MB98 HDJL01 DEC03
HD 10800	27	5.88	4.4	G2V	MB98 BE06 BR06
HD 17206	14	4.47	26.0	F5V	O92 SB91
HD 17848	51	5.25	22.0	A2V	MB98
HD 18978	26	4.08	15.6	A4V	SCBS01
HD 20010	14	3.80	15.0	F8V	O92 WW88
HD 20794	6	4.26	1.5	G8V	DEC03 BE06
HD 21563	182	6.14	37.0	A4V	MB98
HD 22049	3	3.72	6.8	K2V	SB91 WW88 HDJL01 DEC03
HD 22484	14	4.29	4.0	F9V	DEC03 TR08
HD 23362	309	7.91	6.0	K2	SB91
HD 25457	19	5.38	18.0	F5V	DEC03 PAS06 HILL08
HD 28375	118	5.53	12.5	B3V	O92 SB91 TR08
HD 28978	125	5.67	20.7	A2V	BP93
HD 30495	13	5.49	3.6	G3V	HDJL01 DEC03 TR08
HD 31295	37	4.64	11.7	A0V	SN86 WY07
HD 33262	12	4.71	26.6	F7V	BR06 TR08
HD 33636	29	7.00	5.0	G0	BE05 TR08
HD 33949	172	4.36	12.2	B7V	MB98 O92 SB91 PW91 SN86
HD 35850	27	6.30	5.0	F7V	DEC03 PAS06 AP08
HD 36267	88	4.20	16.3	B5V	BP93
HD 37484	60	7.26	5.0	F3V	PAS06 HILL08
HD 38206	69	5.73	3.4	A0V	MB98 DEC03 WY07
HD 38385	53	6.25	9.0	F3V	MB98
HD 38393	9	3.59	10.2	F7V	MB98 HDJL01 SH03 BE06
HD 38678	22	3.55	23.3	A2V	MB98 O92 PW91 AP91 C87 HDJL01 DEC03 SU06 WY07
HD 39014	44	4.34	18.9	A7V	O92 SB91 C87 JU04
HD 39060	19	3.85	13.3	A3V	MB98 O92 C92 SB91 PW91 AP91 WW88 C87 JJE86 HDJL01 DEC03 WY07
HD 40136	15	3.71	18.4	F1V	MB98 BE06b
HD 41700	27	6.35	15.7	G0V	DEC03 HILL08
HD 41742	27	5.93	29.0	F4V	MB98
HD 43955	305	5.51	5.5	B3V	MB98
HD 66591	166	4.81	7.3	B3V	MB98
HD 68456	21	4.74	11.9	F5V	BR06 TR08
HD 69830	13	5.95	1.6	K0V	MB98 BE06 BR06
HD 71043	73	5.89	2.5	A0V	WY07
HD 71155	38	3.91	14.3	A0V	PW91 C87 WY07
HD 75416	97	5.46	4.8	B9V	MB98 SU06 WY07
HD 76151	17	6.01	4.0	G3V	BE06 BR06
HD 79108	115	6.14	10.2	A0V	WY07
HD 80950	81	5.86	15.3	A0V	MB98 WY07
HD 82943	27	6.54	3.0	G0	BE05 TR08
HD 86087	98	5.71	12.0	A0V	BP93
HD 88955	32	3.85	10.5	A2V	MB98
HD 98800	47	8.89	4.6	K4V	MB98 SB91 WW88 MA05
HD 99211	26	4.06	7.3	A9V	MB98
HD 102647	11	2.14	12.4	A3V	O92 C92 SB91 PW91 WW88 C87 HDJL01 DEC03
HD 105211	20	4.14	7.3	F2	BE06b
HD 105686	101	6.16	3.2	A0V	MB98
HD 108257	123	4.82	12.4	B3Vn	BP93
HD 108483	136	3.91	10.9	B3V	MB98
HD 109085	18	4.30	7.3	F2V	MB98 SB91 SH03 BE06b
HD 109573	67	5.78	15.2	A0V	TE00

Table 1. continued.

Star	Distance [pc]	V	$v \sin i$ [km s^{-1}]	Spectral type	Reference
HD 111786	60	6.14	3.6	A0	WY07
HD 113766	131	7.48	5.0	F5V	MB98 O92 CH06
HD 115617	9	4.74	6.4	G5V	BR06
HD 115892	18	2.75	9.0	A2V	MB98 SU06 WY07
HD 117176	18	4.97	4.7	G5V	BE05 BR06
HD 117360	35	6.52	19.3	F6V	MB98
HD 121847	104	5.20	17.5	B8V	MB98 PW91
HD 123160		8.66	7.8	K5	SB91
HD 124771	169	5.06	22.1	B4V	MB98
HD 128311	17	7.48	5.7	K0	BE05 BE06
HD 131885	121	6.91	10.0	A0V	MB98
HD 135344	78	7.91	4.5	F3V	MB98 O92 WW88
HD 136246	143	7.18	2.0	A1V	WY07
HD 139365	136	3.66	11.0	B2.5V	MB98
HD 139664	18	4.64	8.8	F5V	O92 PW91 WW88 HDJL01 DEC03 CH06 BE06b
HD 141569	99	7.11	25.8	B9	O92 SB91 WW88 JJE86 SH03 CL03
HD 142096	109	5.04	17.0	B3V	MB98 O92 SB91
HD 142114	133	4.59	27.3	B2.5V	MB98 O92
HD 142165	127	5.38	23.8	B5V	MB98
HD 144432	253	8.19	8.5	F0V	MB98 O92 WW88
HD 145482	143	4.58	18.5	B2V	MB98
HD 150638	240	6.46	3.5	B8V	PW91
HD 152391	17	6.65	3.0	G8V	DEC03 BR06 TR08
HD 158643	131	4.78	1.7	A0V	O92
HD 158793		8.83	22.5		BP93
HD 159082	152	6.42	25.3	B9.5V	BP93
HD 160691	15	5.12	3.8	G5V	MB98 BE05
HD 161868	29	3.75	21.7	A0V	O92 C87 SN86
HD 164249	47	7.01	21.0	F5V	PW91 DEC03
HD 164577	81	4.42	21.5	A2V	WA95
HD 165341	5	4.03	14.7	K0V	DEC03
HD 166841	214	6.32	29.5	B9V	MB98
HD 169830	36	5.90	4.5	F8V	BE05
HD 176638	56	4.74	2.0	A0V	MB98
HD 177817	274	6.00	13.0	B7V	DEC03
HD 178253	40	4.11	20.5	A0V	MB98 PW91
HD 181296	48	5.03	21.9	A0V	BP93 MB98
HD 181327	51	7.04	18.0	F6V	MB98 SCH06 CH06
HD 181869	52	3.96	8.5	B8V	MB98 WY07
HD 183324	59	5.79	3.6	A0V	WY07
HD 185507	209	5.18	6.4	B3V	BP93 FR96
HD 188228	33	3.97	12.0	A0V	SU06
HD 191089	54	7.18	4.5	F5V	MB98 HILL08 CH06
HD 198160	73	5.67	13.4	A2	RI05
HD 199260	21	5.70	4.3	F7V	BE06b
HD 203608	9	4.21	5.1	F6V	MB98 BE06 BR06
HD 206893	39	6.69	29.0	F5V	DEC03
HD 207129	16	5.57	3.5	G2V	MB98 O92 WW88 O86 HDJL01 DEC03 SH03 TR08
HD 209253	30	6.63	16.0	F7V	DEC03 PAS06 HILL08
HD 216435	33	6.03	5.7	G3V	BP93
HD 216437	27	6.04	4.0	G4V	BE06 BR06
HD 216956	8	1.17	9.5	A3V	MB98 O92 C92 SB91 WW88 C87 HDJL01 DEC03 HO98
HD 221853	71	7.35	8.9	F0	DEC03
HD 224392	49	5.00	20.8	A1V	MB98 O92

Note – The distances, visual magnitudes and spectral sypes are taken from the Hipparcos catalog.
References (alphabetically sorted): AP08 = Apai et al. (2008), BE05 = Beichman et al. (2005), BE06 = Beichman et al. (2006a), BE06b = Beichman et al. (2006b), BP93 = Backman & Paresce (1993), BR06 = Bryden et al. (2006), C87 = Cote (1987), C92 = Cheng et al. (1992), CH06 = Chen et al. (2006), CL03 = Clampin et al. (2003), DEC03 = Decin et al. (2003), FR96 = Friedemann et al. (1996), HDJL01 = Habing et al. (2001), HILL08 = Hillenbrand et al. (2008), HO98 = Holland et al. (1998), JJE86 = Jaschek et al. (1986), JU04 = Jura et al. (2004), MA05 = Mamajek et al. (2005), MB98 = Mannings & Barlow (1998), O92 = Oudmaijer et al. (1992), PAS06 = Pascucci et al. (2006), PW91 = Patten & Willson (1991), RI05 = Rieke et al. (2005), SB91 = Stencel & Backman (1991), SCBS01 = Song et al. (2001), SH03 = Sheret et al. (2003), SCH06 = Schneider et al. (2006), SN86 = Sadakane & Nishida (1986), SU06 = Su et al. (2006), TE00 = Telesco et al. (2000), TR08 = Trilling et al. (2008), WA95 = Waters et al. (1995), WW88 = Walker & Wolstencroft (1988), WY07 = Wyatt et al. (2007a).

Table 2. List of Fe lines used for the metallicity determinations applying the WIDTH program.

Wavelength	log gf	Reference
Fe I		
3927.92	−2.191	K94
4063.59	0.070	FMW
4071.74	−0.022	FMW
4122.64	−7.705	K94
4132.06	−0.650	FMW
4175.64	−0.670	FMW
4184.89	−0.860	FMW
4202.03	−0.708	FMW
4235.94	−0.341	FMW
4247.43	−0.230	FMW
4250.12	−0.405	FMW
4250.79	−0.710	FMW
4260.47	−0.020	FMW
4271.76	−0.164	FMW
4325.76	−0.010	FMW
4383.55	0.200	FMW
4404.75	−0.142	FMW
4415.12	−0.615	FMW
5044.21	−2.150	FMW
5247.05	−4.946	FMW
5322.04	−3.030	FMW
5373.71	−0.860	FMW
5560.21	−1.190	FMW
5576.09	−1.000	FMW
5651.47	−2.000	FMW
5806.73	−1.050	FMW
5814.81	−1.970	FMW
5852.22	−1.330	FMW
5856.09	−1.640	FMW
6065.48	−1.530	FMW
6065.48	−3.910	K94
6105.13	−2.050	FMW
6120.25	−5.950	FMW
6151.62	−3.299	FMW
6157.73	−1.260	FMW
6165.36	−1.550	FMW
6213.43	−2.660	FMW
6229.23	−2.970	FMW
6303.46	−2.660	FMW
6380.74	−1.400	FMW
6430.85	−2.006	FMW
Fe II		
3938.29	−3.890	FMW
4178.86	−2.480	FMW
4491.40	−2.700	FMW
4515.34	−2.480	FMW
4520.22	−2.600	FMW
4541.52	−3.050	FMW
4555.89	−2.290	FMW
4576.33	−3.932	K88
4620.52	−3.280	FMW
4629.34	−2.370	FMW
4666.76	−3.330	FMW
5234.61	−3.785	K88
5234.62	−2.050	FMW
5425.26	−3.360	FMW
6247.56	−2.329	K88
6369.46	−4.253	K88
6416.92	−2.740	K88
6432.68	−1.059	K88
6432.68	−3.708	K88
6442.95	−2.885	K88

References (alphabetically sorted): FMW = Fuhr et al. (1988), K88 = Kurucz (1988), K94 = Kurucz (1994).

Table 3. Temperatures, gravities, microturbulent velocities (ξ), metallicities (average values), dispersions (δ), slope of the [Fe/H] vs. equivalent width plot and number of lines (N) used with the WIDTH9 program, applying the N93 and C97 calibrations for the Vega-like sample.

	N93						C97						
HD number	$T_{\rm eff}$ [K]	log g [dex]	ξ [km s^{-1}]	[Fe/H] [dex]	δ[Fe/H] [dex]	Slope [pm^{-1}] $\times10^{-3}$	$T_{\rm eff}$ [K]	log g [dex]	ξ [km s^{-1}]	[Fe/H] [dex]	δ[Fe/H] [dex]	Slope [pm^{-1}] $\times10^{-3}$	N
105	5914	4.57	1.43	−0.37	0.26	5.0	5936	4.54	1.24	−0.33	0.26	2.2	15
142	6065	4.23	1.13	−0.45	0.27	3.1	6278	4.22	1.23	−0.27	0.25	3.9	20
2623	4937	4.10	0.91	−0.20	0.26	2.5	4931	4.07	0.50	0.09	0.20	7.9	23
3003	8823	4.21	1.82	0.17	0.22	2.3	8844	3.85	2.03	0.07	0.31	7.1	17
9672	8931	4.17	1.79	−0.32	0.26	5.9	8867	4.09	1.85	−0.31	0.21	0.9	24
10647	5946	4.60	1.30	0.12	0.22	7.5	5863	4.37	1.10	−0.07	0.28	4.7	29
10700	5350	5.01	0.96	−0.73	0.29	4.0	5463	3.96	0.87	−0.67	0.23	4.5	17
10800	5912	4.91	1.35	0.16	0.27	6.0	5862	4.12	1.05	0.12	0.26	3.1	30
17206	6348	4.46	1.47	−0.22	0.27	8.6	6185	4.11	1.28	0.03	0.21	2.5	22
17848	8258	4.07	2.74	−0.02	0.28	5.6	8215	3.43	2.93	−0.17	0.20	4.7	21
18978	7975	4.03	3.01	−0.39	0.25	2.0	8144	3.87	3.06	−0.11	0.23	9.7	22
20010	6094	4.09	1.28	−0.64	0.20	6.8	6226	3.77	1.51	−0.62	0.30	6.2	27
20794	5579	4.78	0.97	−0.17	0.29	3.2	5602	4.07	0.95	−0.58	0.24	4.0	17
21563	6818	4.22	1.57	−0.41	0.30	4.0	6624	4.19	1.74	−0.10	0.26	5.4	19
22049	5039	3.92	0.55	−0.08	0.25	4.3	4910	3.89	0.85	−0.13	0.27	1.6	22
22484	5991	4.18	1.37	−0.22	0.28	6.4	5911	4.51	1.34	−0.19	0.26	3.6	21
23362	4995	4.21	0.72	−0.07	0.25	4.4	4773	4.18	0.62	−0.47	0.29	5.3	25
25457	6435	4.68	1.55	0.18	0.21	5.7	6515	4.25	1.59	−0.22	0.22	2.8	29
28375	15 180	4.30	0.19	0.10	0.29	6.9	15 172	4.35	0.10	−0.19	0.26	4.5	23
28978	9050	4.24	1.69	0.20	0.22	8.3	9050	3.48	1.66	0.33	0.24	5.5	18
30495	5611	4.60	1.04	0.11	0.29	2.7	5655	3.98	0.96	0.13	0.24	6.4	23
31295	8633	4.09	2.13	−0.68	0.24	2.8	8479	3.59	2.07	−0.76	0.25	5.7	27
33262	6212	4.71	1.30	0.07	0.25	4.6	6089	4.44	1.14	−0.09	0.24	3.9	27
33636	5622	4.46	1.14	0.03	0.20	7.2	5640	4.00	1.04	−0.09	0.27	6.0	16
33949	12 490	3.48	0.14	0.00	0.21	3.6	12 553	3.59	0.10	−0.23	0.27	7.9	19
35850	6170	4.70	1.21	−0.23	0.27	2.7	6075	4.41	1.52	−0.12	0.24	4.0	26
36267	14 748	4.36	0.07	−0.23	0.23	2.5	14 885	4.40	0.10	−0.02	0.23	6.3	21
37484	6323	4.54	1.67	−0.17	0.31	2.5	6312	4.51	1.20	−0.25	0.30	2.5	28
38206	10 281	4.42	0.10	−0.06	0.21	2.8	10 165	4.34	0.39	0.32	0.23	4.3	23
38385	6867	3.98	1.79	0.09	0.25	2.2	6558	3.57	1.80	0.12	0.30	1.3	24
38393	6199	4.43	1.22	0.30	0.21	4.4	6317	4.29	1.25	0.21	0.27	3.2	26
38678	8197	4.06	2.94	−0.13	0.21	6.2	8475	3.40	2.91	−0.35	0.28	4.9	29
39014	7555	3.50	2.28	−0.41	0.26	6.5	7582	3.59	2.53	−0.39	0.30	4.9	23
39060	8157	4.23	3.05	0.00	0.29	5.0	7995	3.95	2.78	0.17	0.21	5.7	16
40136	6998	4.10	1.69	−0.27	0.30	7.3	6890	3.91	1.94	−0.33	0.27	6.3	29
41700	6012	4.56	1.03	−0.14	0.22	4.2	5973	4.37	1.38	−0.41	0.22	3.2	23
41742	6292	4.65	1.65	−0.31	0.28	9.6	6208	4.23	1.47	−0.30	0.30	2.2	16
43955	17 893	4.12	0.10	−0.15	0.26	4.4	17 922	5.19	0.10	−0.20	0.26	5.9	21
66591	16 753	4.08	0.10	0.04	0.25	6.3	16 787	4.15	0.06	−0.09	0.21	1.3	23
68456	6274	4.20	1.16	−0.36	0.26	9.8	6289	3.08	1.48	−0.20	0.24	7.5	21
69830	5442	5.09	0.91	−0.07	0.23	7.0	5599	4.05	1.13	−0.06	0.29	7.8	24
71043	10 138	4.20	0.51	0.19	0.25	8.3	10 215	4.31	0.48	−0.14	0.25	1.9	23
71155	9945	4.11	0.79	−0.11	0.26	2.6	9929	4.18	0.64	0.25	0.21	7.2	21
75416	12 602	4.23	0.10	0.10	0.28	8.3	12 461	4.25	0.10	0.01	0.26	6.7	24
76151	5728	4.52	0.86	−0.07	0.26	9.0	5868	3.59	0.95	−0.07	0.22	0.4	22
79108	10 135	4.02	0.49	−0.10	0.28	3.0	10 107	4.11	0.22	−0.26	0.22	1.8	16
80950	10 381	4.45	0.34	−0.29	0.31	5.2	10 496	4.36	0.35	−0.28	0.20	2.5	18
82943	5913	4.15	1.44	0.35	0.30	5.8	5659	3.55	1.33	0.32	0.22	7.8	28
86087	9455	4.32	1.27	0.27	0.24	1.7	9396	4.34	1.38	−0.07	0.28	5.2	29
88955	8742	4.00	2.17	−0.14	0.30	4.9	8857	3.90	2.32	0.12	0.29	8.5	16
98800	4484	3.99	0.50	−0.05	0.25	5.2	4479	3.96	0.29	−0.24	0.23	3.7	23
99211	10 684	3.95	0.07	−0.15	0.25	5.6	10 510	5.45	0.13	0.14	0.23	3.3	26
102647	8443	4.17	2.60	−0.24	0.20	1.2	8529	4.07	2.63	−0.07	0.27	8.6	27
105211	6974	4.08	1.91	−0.36	0.22	2.7	6914	3.91	1.86	−0.04	0.26	3.0	18
105686	9954	4.26	0.62	−0.72	0.29	2.1	9989	4.25	0.67	−0.39	0.27	0.2	13
108257	16 663	4.06	0.10	−0.38	0.24	6.3	16 667	4.14	0.10	−0.36	0.21	9.2	16

Table 3. continued.

	N93						C97						
HD number	$T_{\rm eff}$ [K]	log g [dex]	ξ [km s^{-1}]	[Fe/H] [dex]	δ[Fe/H] [dex]	Slope [pm^{-1}] $\times10^{-3}$	$T_{\rm eff}$ [K]	log g [dex]	ξ [km s^{-1}]	[Fe/H] [dex]	δ[Fe/H] [dex]	Slope [pm^{-1}] $\times10^{-3}$	N
108483	20 406	4.36	0.13	0.02	0.21	2.6	20338	4.55	0.19	0.14	0.25	5.4	20
109085	6734	4.27	1.68	−0.20	0.24	1.8	6611	4.08	1.41	−0.23	0.27	6.4	20
109573	9305	4.32	1.38	−0.06	0.31	2.8	9437	4.36	1.54	0.10	0.30	5.7	15
111786	8075	3.90	2.67	−1.42	0.30	3.8	8090	3.84	2.71	−1.65	0.22	5.4	24
113766	6843	4.35	1.51	0.06	0.23	7.4	6870	4.17	1.57	−0.14	0.27	4.6	16
115617	5506	4.51	0.75	0.20	0.29	4.2	5427	3.54	0.81	0.13	0.24	5.3	16
115892	8658	4.05	2.36	−0.29	0.27	3.3	8526	3.66	2.43	−0.33	0.28	3.2	14
117176	5351	4.01	0.95	0.01	0.26	5.4	5348	3.28	0.77	−0.12	0.26	6.5	25
117360	6169	4.46	1.39	−0.39	0.21	8.1	6275	4.28	1.10	−0.61	0.26	8.3	25
121847	12 556	4.02	0.16	−0.30	0.26	2.5	12461	4.07	0.10	0.10	0.27	4.4	16
123160	4297	4.10	0.18	0.27	0.27	1.8	4465	4.07	0.50	0.17	0.25	7.3	28
124771	16 042	4.09	0.21	0.15	0.21	5.3	16 133	4.16	0.10	0.01	0.21	9.2	29
128311	4583	4.82	0.31	0.16	0.24	5.8	4763	2.94	0.66	0.04	0.29	2.3	16
131885	9633	4.20	1.01	−0.44	0.29	5.1	9817	4.17	1.23	−0.19	0.28	7.1	23
135344	6696	4.21	1.80	−0.37	0.21	5.8	6657	3.94	1.49	−0.41	0.28	1.4	20
136246	9782	4.30	1.02	−0.29	0.23	5.0	9903	4.27	0.88	−0.49	0.28	3.5	27
139365	18 136	4.41	0.24	0.02	0.25	1.9	17 920	4.30	0.23	0.35	0.29	6.5	26
139664	6576	4.49	1.53	−0.46	0.28	2.4	6578	4.28	1.73	−0.08	0.26	3.1	24
141569	9953	4.05	0.43	−0.32	0.27	3.7	9826	3.96	0.43	−0.01	0.20	8.7	18
142096	17 132	4.66	0.10	−0.28	0.28	6.8	17 201	4.62	0.25	−0.16	0.23	9.2	14
142114	18 469	4.48	0.10	0.09	0.26	5.4	18 262	5.33	0.10	0.06	0.26	1.1	21
142165	14 081	4.33	0.10	−0.03	0.23	5.7	13 955	5.77	0.10	0.10	0.30	6.7	20
144432	6857	3.66	1.56	−0.19	0.23	9.5	6924	3.63	1.81	−0.13	0.28	0.4	25
145482	19 247	4.24	0.14	−0.38	0.27	4.3	19 331	4.68	0.10	−0.19	0.25	4.2	20
150638	12 394	4.26	0.11	−0.34	0.23	2.8	12 520	4.28	0.10	−0.52	0.22	2.8	22
152391	5347	4.94	1.00	−0.24	0.26	1.2	5263	3.55	0.91	−0.26	0.31	2.2	27
158643	9636	3.11	0.97	−0.44	0.22	3.2	9667	3.32	0.86	−0.20	0.30	5.6	26
158793	9921	3.11	0.66	0.25	0.25	3.6	9862	3.32	0.87	0.37	0.24	8.3	16
159082	10 886	4.02	0.02	0.09	0.31	4.7	11 064	3.97	0.19	−0.22	0.24	1.7	26
160691	5463	4.30	0.95	−0.07	0.25	4.5	5662	4.27	1.15	−0.06	0.21	1.1	21
161868	8526	3.96	2.18	0.11	0.30	7.3	8677	3.79	2.40	−0.26	0.28	5.3	26
164249	6765	4.44	1.61	−0.04	0.22	7.9	6738	3.09	1.76	−0.04	0.23	6.2	29
164577	9627	3.66	1.30	−0.14	0.24	6.9	9790	3.53	1.08	−0.37	0.24	6.7	24
165341	5114	4.20	0.60	−0.26	0.30	0.8	5082	4.17	0.84	−0.38	0.26	7.2	26
166841	10 909	3.43	0.10	−0.16	0.31	0.7	11 033	3.33	0.14	0.05	0.27	4.7	16
169830	6234	4.12	1.16	−0.15	0.23	4.3	6261	3.80	1.55	0.31	0.25	1.6	26
176638	10 223	3.99	0.34	−0.21	0.23	2.3	10 155	3.97	0.13	−0.05	0.28	5.7	21
177817	12 754	3.62	0.02	0.13	0.27	4.2	12 537	3.77	0.10	0.04	0.21	3.0	26
178253	8402	3.98	2.58	0.12	0.23	9.9	8273	4.35	2.37	−0.26	0.22	6.3	23
181296	9138	4.24	1.85	0.06	0.30	3.0	9045	4.31	1.77	0.14	0.28	1.0	21
181327	6332	4.54	1.52	0.34	0.23	4.1	6561	4.19	1.51	0.24	0.28	2.5	27
181869	12 018	4.11	0.10	−0.02	0.28	5.8	12 049	4.11	0.16	−0.03	0.29	0.7	19
183324	10 373	4.18	0.13	−1.13	0.27	7.6	10 224	4.17	0.35	−1.29	0.30	3.5	21
185507	21 389	3.96	0.10	−0.14	0.27	4.0	21 481	4.59	0.10	−0.07	0.21	2.0	31
188228	10 444	4.29	0.10	−0.17	0.25	0.2	10 312	4.23	0.28	−0.02	0.31	6.4	17
191089	6323	4.43	1.58	−0.41	0.25	1.4	6332	4.09	1.55	−0.17	0.29	7.8	24
198160	7817	3.91	3.02	−0.78	0.29	7.3	7928	4.02	2.92	−0.99	0.24	5.4	25
199260	6120	4.65	1.14	−0.26	0.28	5.0	6134	4.37	1.38	−0.01	0.31	5.1	18
203608	6203	4.66	1.61	−0.43	0.28	7.0	6107	4.42	1.58	−0.72	0.24	3.7	19
206893	6587	4.40	1.39	−0.07	0.27	8.5	6366	4.37	1.35	0.20	0.23	4.3	24
207129	5838	4.41	1.33	−0.26	0.20	3.8	5899	3.65	1.35	−0.22	0.27	1.0	26
209253	6208	4.65	1.13	0.02	0.27	6.5	6044	4.40	1.58	−0.26	0.26	6.8	16
216435	5687	3.84	1.09	0.07	0.26	9.2	5899	5.23	1.27	−0.17	0.25	6.5	22
216437	5709	4.04	1.21	0.34	0.21	5.6	5727	5.37	1.18	0.27	0.28	5.9	21
216956	8762	4.18	2.28	−0.42	0.28	4.8	8729	4.87	1.84	−0.22	0.20	2.0	22
221853	6213	4.02	1.24	−0.18	0.24	2.8	6082	3.99	1.48	0.08	0.26	3.5	15
224392	8885	4.12	1.82	0.09	0.21	1.4	8712	4.10	2.09	0.14	0.27	2.7	23

Table 4. $T_{\rm eff}$, $\log g$ and [Fe/H] derived using the Downhill method, for the sample of Vega-like stars.

Star	$T_{\rm eff}$ [K]	$\log g$	[Fe/H]
HD 105	5989	4.57	−0.13
HD 142	6182	4.12	−0.21
HD 2623	4923	4.10	−0.15
HD 3003	8794	4.10	0.06
HD 9672	8865	4.21	−0.12
HD 10647	5954	4.67	−0.01
HD 10700	5499	4.97	−0.53
HD 10800	5901	4.84	0.09
HD 17206	6359	4.57	−0.14
HD 17848	8308	3.96	−0.05
HD 18978	8050	4.14	−0.25
HD 20010	6072	4.07	−0.39
HD 20794	5629	4.70	−0.35
HD 21563	6714	4.22	−0.25
HD 22049	4963	3.92	−0.17
HD 22484	5943	4.29	−0.17
HD 23362	4899	4.21	−0.23
HD 25457	6364	4.68	0.00
HD 28375	15 275	4.20	−0.02
HD 28978	9075	4.26	0.17
HD 30495	5759	4.53	0.01
HD 31295	8651	4.11	−0.75
HD 33262	6073	4.83	−0.10
HD 33636	5744	4.56	−0.08
HD 33949	12 459	3.44	−0.07
HD 35850	6021	4.66	−0.05
HD 36267	14 760	4.27	−0.01
HD 37484	6380	4.54	−0.22
HD 38206	10 135	4.36	0.14
HD 38385	6726	3.87	0.02
HD 38393	6163	4.37	0.08
HD 38678	8327	3.97	−0.19
HD 39014	7489	3.41	−0.40
HD 39060	8036	4.21	0.11
HD 40136	7007	4.12	−0.32
HD 41700	6079	4.55	−0.22
HD 41742	6331	4.61	−0.33
HD 43955	17 890	4.12	−0.15
HD 66591	16 641	4.15	−0.19
HD 68456	6305	4.14	−0.39
HD 69830	5586	5.15	0.16
HD 71043	10 103	4.31	−0.02
HD 71155	9881	4.22	0.14
HD 75416	12 603	4.25	0.16
HD 76151	5750	4.46	−0.16
HD 79108	10 273	4.11	−0.07
HD 80950	10 330	4.36	−0.05
HD 82943	5764	4.25	0.30
HD 86087	9310	4.25	0.08
HD 88955	8707	4.04	−0.02
HD 98800	4595	3.99	−0.22
HD 99211	10 625	4.90	−0.01
HD 102647	8522	4.26	−0.25
HD 105211	6901	3.91	−0.29
HD 105686	9930	4.19	−0.48
HD 108257	16 576	3.98	−0.53
HD 108483	20 320	4.33	−0.06
HD 109085	6756	4.17	−0.21
HD 109573	9378	4.43	−0.03
HD 111786	8115	3.84	−1.45

Table 4. continued.

Star	$T_{\rm eff}$ [K]	log g	[Fe/H]
HD 113766	6796	4.32	0.09
HD 115617	5558	4.55	0.07
HD 115892	8600	4.11	−0.46
HD 117176	5495	4.02	−0.08
HD 117360	6314	4.51	−0.45
HD 121847	12 472	4.00	−0.09
HD 123160	4356	4.10	0.04
HD 124771	16 136	4.18	−0.02
HD 128311	4635	4.71	−0.04
HD 131885	9680	4.20	−0.23
HD 135344	6692	4.11	−0.20
HD 136246	9790	4.30	−0.28
HD 139365	17 990	4.33	0.17
HD 139664	6693	4.55	−0.31
HD 141569	9963	4.11	−0.07
HD 142096	17 034	4.75	−0.27
HD 142114	18 429	4.42	0.23
HD 142165	14 077	4.31	0.11
HD 144432	6957	3.55	−0.18
HD 145482	19 214	4.32	−0.24
HD 150638	12 453	4.16	−0.42
HD 152391	5418	5.05	−0.12
HD 158643	9772	3.12	−0.25
HD 158793	9781	3.03	0.32
HD 159082	10 990	3.91	−0.06
HD 160691	5600	4.30	0.09
HD 161868	8567	3.98	−0.06
HD 164249	6620	4.32	−0.09
HD 164577	9687	3.67	−0.29
HD 165341	5153	4.20	−0.32
HD 166841	10 885	3.36	−0.02
HD 169830	6349	4.08	0.08
HD 176638	10 095	4.10	−0.21
HD 177817	12 667	3.72	0.19
HD 178253	8448	4.01	−0.11
HD 181296	9207	4.30	0.17
HD 181327	6449	4.44	0.29
HD 181869	12 100	4.00	0.18
HD 183324	10 325	4.17	−1.24
HD 185507	21 374	4.59	0.04
HD 188228	10 366	4.23	−0.13
HD 191089	6402	4.33	−0.34
HD 198160	7860	4.02	−1.03
HD 199260	6231	4.37	−0.11
HD 203608	6105	4.61	−0.51
HD 206893	6454	4.40	−0.05
HD 207129	5776	4.39	−0.12
HD 209253	6175	4.62	−0.17
HD 216435	5755	3.82	−0.17
HD 216437	5757	3.99	0.20
HD 216956	8743	4.09	−0.34
HD 221853	6196	4.02	0.00
HD 224392	8778	4.06	0.07